Pathology

Note

Distinct malignant epithelial tumors associated with *Felis catus* papilloma virus type 3 and type 4 co-infection in a domestic cat

Hinata Abe [1, #], Nanami X Kato [2, #], Mika Tanabe [3], Taichi Shimabukuro [4], Saki Hashimoto [5], Takuya Hirai [1,6], Naoyuki Fuke [1, *], Akatsuki Saito [2,6,7, *]

[1] Laboratory of Veterinary Pathology, Department of Veterinary Science, Faculty of Agriculture, University of Miyazaki, Miyazaki, Miyazaki 889-2192, Japan

[2] Laboratory of Veterinary Microbiology, Department of Veterinary Science, Faculty of Agriculture, University of Miyazaki, Miyazaki, Miyazaki 889-2192, Japan

[3] Veterinary Pathology Diagnostic Center, Nakama, Fukuoka, 809-0011, Japan

[4] Ryukyu Animal Medical Center, Tomigusuku, Okinawa, 901-0224, Japan

[5] Saki Animal Hospital, Fukuoka, Fukuoka, 815-0035, Japan

[6] Graduate School of Medicine and Veterinary Medicine, University of Miyazaki, Miyazaki, Miyazaki 889-1692, Japan

[7] Center for Animal Disease Control, University of Miyazaki, Miyazaki, Miyazaki 889-2192, Japan

[#] These authors contributed equally.

* Corresponding author: Akatsuki Saito (sakatsuki@miyazaki-u.ac.jp) or Naoyuki Fuke (fuke.naoyuki.z2@miyazaki-u.ac.jp)

Running Head: FCAPV3 AND FCAPV4 IN FELINE CARCINOMAS

Abstract

A 12-year-8-month-old neutered male American Shorthair cat presented with multiple nail bed masses and an ulcerative lip lesion. PCR identified *Felis catus* papillomavirus type 3 (FcaPV3) in the nail masses and type 4 (FcaPV4) in the lip lesion. Histopathology revealed basosquamous cell carcinoma (BSCC) in the digits and Bowenoid *in situ* carcinoma (BISC) in the lip. Tumor cells showed strong p16 positivity and weak or negative pRb and p53 expression. *In situ* hybridization confirmed FcaPV3 and FcaPV4 *E6* genes in digital and lip tumors, respectively. Over six months, viral sequencing showed 23 nucleotide changes in FcaPV3, suggesting viral evolution. This is the first report of distinct malignant epithelial tumors independently induced by FcaPV3 and FcaPV4 in a cat.

Keywords

Basosquamous cell carcinoma, Bowenoid *in situ* carcinoma, Co-infection, *Felis catus* papillomavirus

Papillomaviruses (PVs) are small, non-enveloped viruses with circular double-stranded DNA genomes [17]. They infect epithelial and mucosal tissues [1, 21] and are known to cause viral lesions as well as malignant epithelial tumors, including Bowen's disease (Bowenoid *in situ* carcinoma; BISC), squamous cell carcinoma (SCC), and basal cell carcinoma (BCC) [1, 18, 19, 22]. Because of their strict host specificity, PVs are named after the host species from which they are isolated [17, 22].

Human PVs enter the host through microabrasions in the epithelium or mucosa, infecting basal keratinocytes [5]. After infection, the viral genome is transported to the nucleus, where it remains as an episome. The genome replicates in synchrony with host cell division and is inherited by daughter cells [15, 24]. Expression of late genes encoding capsid proteins begins in the spinous layer, followed by virion assembly in the granular layer. Mature virions then accumulate and are released from the cornified or non-keratinized epithelial layers [5, 8, 17, 20].

Compared to human PVs, the mechanisms underlying PV-induced malignancies in animals remain poorly understood. In humans, expression of the *E1* and *E2* genes facilitates limited viral replication, allowing infection of adjacent basal cells and persistence of the virus within the epithelium [20]. When viral DNA integrates into the host genome, persistent expression of the viral oncogenes *E6* and *E7* occurs [6]. These oncoproteins promote tumorigenesis by degrading and inactivating host tumor suppressors p53 and pRB, respectively [2, 25, 27].

In cats, *Felis catus* PVs (FcaPV) have been increasing associated with malignant epithelial tumors such as SCC. To date, six distinct FcaPV types have been identified [16, 18, 21]. Each FcaPV type shows a distinct tissue tropism and tumor-inducing potential, suggesting that infection site specifically may play an important role in feline-PV-associated oncogenesis.

FcaPV1 infects both the skin and oral mucosa and is associated with the development of cutaneous and oral papillomas, viral plaques, and BISC [16]. FcaPV2 primarily infects the skin and has been associated with the development of SCC and BCC [16]. FcaPV3 mainly targets the skin and is associated with viral plaques, BISC, SCC, and other skin tumors. FcaPV4 preferentially infects the lips and is associated with BISC development [7, 14]. FcaPV5 predominately detected in the skin and is associated with viral plaques and BISC, while FcaPV6 infects the nasal planum and is associated with SCC [16].

Although co-infections with multiple PV types have been reported in humans [23, 28], dogs [12], cattle [3, 26], and porcupines [13], such cases have not been documented in cats. Here, we describe a feline case in which different FcaPV types were detected in malignant epithelial tumors of the nail bed and lips. The case was analyzed pathologically and virologically to determine tumor characteristics, FcaPV types, and their tissue localization.

A 12-year-8-month-old neutered male American Shorthair cat, negative for feline immunodeficiency virus and feline leukemia virus, had a history of chronic nail-biting of the left forelimb since around 2021 and was treated for paronychia in 2022. In April 2023, nail bed masses developed on the right forelimb and left hindlimb. Radiographs revealed osteolysis of the second digit of the right forelimb, while computed tomography showed no evidence of pulmonary or metastatic lesions. Histopathological examination by a commercial diagnostic service identified the nail bed masses on the right first and second digits, left first and second digits, and left second hind digit as malignant epithelial tumors.

In June 2023, multiple nail bed masses were observed on the right first digit, left second digit, and left second hind digit **(Fig. 1A**). These were surgically amputated, and the excised tissues were submitted to the Veterinary Pathology Diagnostic Center and the Laboratory of Veterinary Pathology, University of Miyazaki, for histopathological evaluation. In January 2024, a new inflammatory lesion was detected in the nail bed of the right second digit (**Fig. 1B**), along with an ulcerative lesion on the left lip (**Fig. 1C**). Both lesions were surgically excised—either in June 2023 or January 2024—and submitted to our laboratory for pathological examination in August 2023 and February 2024, respectively.

Virological analyses were conducted using multiple nail bed masses, a single nail bed lesion, and a lip lesion excised in June 2023 and January 2024, respectively. Genomic DNA was extracted from each fresh-frozen tissue sample using the DNeasy Blood & Tissue Kit (QIAGEN, Venlo, Netherlands; Catalog no. 69506), following the manufacturer's instructions.

Real-time PCR was performed with the KAPA SYBR Fast qPCR Kit (ROX Low; NIPPON Genetics, Tokyo, Japan; Catalog no. KK4621) according to the manufacturer's protocol. Each 12.5 μL reaction mixture contained 0.05 μL of each primer (50 μM forward and reverse), 6.25 μL of KAPA SYBR FAST qPCR Master Mix (2×), 4.15 μL nuclease-free water, and 2 μL of genomic DNA. The primers used are listed in **Supplemental Table 1A**. Amplification was carried out on a QuantStudio 3 real-time PCR

system (Life Technologies Japan, Inc., Tokyo, Japan) with the following thermal cycling conditions: 95°C for 3 min, followed by 40 cycles of 95°C for 3 sec and 60°C for 20 sec. Nuclease-free water was used as a no-template negative control in all reactions.

Amplification of the *Felis catus Alb* gene was used as an internal control to verify DNA quality and PCR efficiency. Consistent amplification of the *Alb* gene across all samples confirmed that DNA quality and quantity were adequate for viral detection.

In multiple nail bed masses collected in August 2023, the mean Ct value for FcaPV3 was 12.7, lower than those of other FcaPV types (**Fig. 2**). Similarly, the single nail bed lesion collected in February 2024 showed the mean Ct value of 14.4 for FcaPV3, also lower than other FcaPV types (**Fig. 2**). The lip lesion collected in February 2024 showed the mean Ct value of 19.9 for FcaPV4, which was lower than those of other FcaPV types (**Fig. 2**). These real-time PCR findings indicated FcaPV3 infection in the nail bed lesions and FcaPV4 infection in the lip lesions (**Fig. 2**).

To determine the viral genome sequence, PCR amplification of FcaPV genomic DNA was performed using PrimeSTAR® GXL DNA Polymerase (TaKaRa Bio Inc., Shiga, Japan, Catalog no. R050A) according to the manufacturer's instructions. Each 50 μL reaction mixture contained 0.2 μL of each primer (50 μM), 10 μL 5× PrimeSTAR GXL Buffer, 4 μL of dNTP Mixture (2.5 mM each), 33.6 μL of nuclease-free water, 1 μL of PrimeSTAR GXL DNA Polymerase, and 1 μL of genomic DNA. The primers used for sequencing are listed in **Supplementary Table 1B**. PCR conditions were as follows: initial denaturation at 98°C for 10 s, followed by 35 cycles of 98°C for 10 s, 60°C for 15 s, and 68°C for 40 s, with a final extension at 68°C for 7 min. Nuclease-free water was used as a negative control in all experiments.

PCR products were separated by electrophoresis on a 1% agarose gel, and specific bands were excised (**Supplementary Figs. 1A-B**). DNA was purified from the gel using the QIAquick Gel Extraction Kit (QIAGEN, Catalog no. 28706).

For Sanger sequencing, PCR products were subjected to cycle sequencing using the SupreDye v3.1 Cycle Sequencing Kit (M&S TechnoSystems, Osaka, Japan, Catalog no. 063002), following the manufacturer's protocol. Each 10 μL sequencing reaction contained 1 μL of primer (1.6 μM), 1 μL of

SupreDye Ready-Reaction Premix, 1.5 μL of 5× Sequencing Buffer, 5.5 μL nuclease-free water, and 1 μL of the PCR product. Thermal cycling conditions included an initial denaturation at 96°C for 10 s, followed by 25 cycles of 96°C for 10 s and 60°C for 4 min. Sequencing products were purified using Gel Filtration Cartridges (M&S TechnoSystems, Catalog no. 42453) and analyzed on a SeqStudio Genetic Analyzer (Life Technologies Japan, Inc.).

Sequence data were processed and analyzed using BioEdit (Informer Technologies, Inc., Wilmington, USA) and MEGA11 (MEGA Software, Tempe, USA). A phylogenetic tree was constructed using full-length genome sequences obtained from GenBank (**Figs. 3A and B**). Multiple sequence alignment was performed using the MUSCLE algorithm in MEGA 11, and phylogenetic relationships were inferred using the maximum likelihood and neighbor-joining methods with the Jones–Taylor–Thornton matrix-based model.

The *FcaPV3/GNGN3/Fukuoka/Japan/2023* strain (GenBank accession number LC859345.2) detected from multiple nail bed masses in August 2023 showed 99.89% nucleotide identity with the reference FcaPV3 strain (GenBank accession number NC_021472.1) (**Supplementary Table 3A**).

The *FcaPV3/cat/Japan/Fukuoka_GNGN3/2024* strain (GenBank accession number LC884935.1), detected in the single nail bed lesion collected in February 2024, showed the highest nucleotide identity (99.92%) with the *FcaPV3/China/SMU-D21/2019* (GenBank accession number ON226485.1) (**Supplementary Table 3B**).

Similarly, the *FcaPV4/Japan/GNGN4/2024* strain (GenBank accession number LC859344.1), identified from a lip lesion collected in February 2024, showed the highest sequence identity (98.59%) with the *FcaPV4/13136* strain (GenBank accession number LC333412.2) (**Supplementary Table 3C**).

Longitudinal sequence comparison between *FcaPV3/GNGN3/Fukuoka/Japan/2023* (detected in multiple nail bed masses collected in August 2023) and *FcaPV3/cat/Japan/Fukuoka_GNGN3/2024* (from a single nail bed lesion collected in February 2024) revealed 23 nucleotide substitutions across the 7,583-base genome (**Fig. 3C**). The substitutions included five C-to-T changes, four T-to-C changes, four A-to-G changes, three G-to-A changes, two each of T-to-A, C-to-G, and A-to-T changes, and one A-to-C substitution.

For histopathological analysis, tissue specimens were fixed in 10% neutral-buffered formalin, embedded in paraffin, sectioned at 4 μm, and stained with hematoxylin and eosin (HE).

Multiple nail bed masses observed in the second digit of the left forelimb, the first digit of the right forelimb, and the second digit of the left hindlimb showed infiltrative neoplastic growth extending from the dermis of the nail bed into the subcutaneous tissue and phalanges **(Fig. 4A)**. The neoplastic tissue was arranged in islands, cords, and trabeculae, with focal squamous differentiation characterized by polygonal cells containing eosinophilic cytoplasm and central keratinization **(Fig. 4B)**. Tumor cells were basaloid to cuboidal, with oval nuclei, coarse chromatin, and one or occasionally two prominent nucleoli. Koilocytes with perinuclear vacuolation were observed **(Fig. 4C)**, along with areas of necrosis, stromal fibrosis, and bone lysis. Some squamous cells were enlarged, containing large nuclei with basophilic, rod-shaped to amorphous cytoplasmic inclusions **(Fig. 4D)**. The mitotic count was 32 per 10 high-power fields (HPFs; 2.37 mm^2). Based on these features, the lesions were diagnosed as basosquamous cell carcinoma (BSCC).

In the single nail bed lesion, the dermis was infiltrated by neutrophils and lymphocytes, with accompanying hemorrhage and fibrin deposition. Epidermal hyperplasia was present, but no neoplastic proliferation was identified. These findings were consistent with onychomycosis.

In the ulcerative lesion of the left lip, well-demarcated neoplastic proliferation was observed within the epidermis, extending into the superficial dermis **(Fig. 4E)**. The neoplastic tissue was subdivided by fibrous connective tissue and remained confined above the basement membrane, exhibiting diffuse intraepithelial growth. Tumor cells were irregularly shaped with indistinct borders, round to pleomorphic nuclei containing finely granular chromatin, and one or two variably sized nucleoli **(Fig. 4F)**. Clear to grayish-blue intranuclear inclusions were evident in tumor cells **(Fig. 4G)**. Some cells contained melanin pigment, showed bluish-gray cytoplasmic swelling **(Fig. 4H)**, or exhibited perinuclear clearing. The mitotic count was 84 per 10 HPFs. Based on these histopathological features, the lesion was diagnosed as BISC.

Immunohistochemistry (IHC) was performed on both BSCC and BISC specimens using the primary antibodies listed in **Supplementary Table 2**. The Histofine Simple Stain MAX-PO™ (MULTI) system (Nichirei Bioscience, Tokyo, Japan) was used as the secondary antibody. For antigen retrieval, sections

stained for p16 were treated in a pH 9.0 buffer, whereas those for p53, p63, and pRb were treated in a pH 6.0 buffer. Primary antibody incubation was conducted at 37°C for 1 hour, followed by incubation with the secondary antibody at 37°C for 40 min. Immunoreactivity was visualized using 3,3′-diaminobenzidine (DAB; Sigma Aldrich, Tokyo, Japan, catalog no. D5637) as the chromogen, and sections were counterstained with hematoxylin.

Both BSCC and BISC neoplastic cells were strongly positive for p16 and p63 (**Figs. 5A–D**) and weakly positive for pRb (**Figs. 5E and F**). The neoplastic cells in BSCC were negative for p53 **(Fig. 5G)**, whereas those in BISC showed positive immunoreactivity for p53 **(Fig. 5H)**.

Similarly, *in situ* hybridization (ISH) was performed on BSCC and BISC tissues using the RNAscope™ 2.5 HD Reagent Kit-BROWN (Cosmo Bio, Tokyo, Japan, catalog no. 322300) according to the manufacturer's instructions, with reference to a previous report [33]. Probes complementary to the E6 gene regions of FcaPV3 and FcaPV4 were designed for this experiment (**Supplementary Table 4**). Sections were first treated with the hydrogen peroxide solution provided in the kit for 10 min at room temperature, rinsed with distilled water, and subjected to heat-induced target retrieval in Target Retrieval Buffer at 105°C for 10 min. The target-specific probes were then hybridized to each section at 40°C for 2 h. Hybridization signals were visualized using DAB for 10 min at room temperature, and sections were counterstained with hematoxylin.

In BSCC, the *FcaPV3 E6* gene was detected in both the nuclei and cytoplasm of tumor cells in a punctate pattern **(Fig. 6A)**. In BISC, the *FcaPV4 E6* gene was similarly detected in the nuclei and cytoplasm of tumor cells **(Fig. 6B)**. Neither *FcaPV3 E6* nor *FcaPV4 E6* was detected in the normal tissues surrounding the BSCC or BISC lesions.

To date, six types of FcaPV have been reported: FcaPV1, FcaPV2, FcaPV3, FcaPV4, FcaPV5, and FcaPV6 [16, 18, 21]. These viruses show site-specific infection patterns and tumor associations depending on the viral type [16]. FcaPV3 predominantly infects the skin, where it is associated with viral plaques, BISC, SCC, and other cutaneous tumors. In contrast, FcaPV4 primarily infects the oral cavity and is linked to stomatitis and BISC [16].

In the present case, FcaPV3 was detected in nail bed masses from the first digit of the right forelimb, the second digit of the left forelimb, and the second digit of the left hindlimb in June 2023, as well as in

200 an inflammatory nail bed lesion of the second digit of the right forelimb in January 2024. FcaPV4 was
201 detected in a lip lesion that appeared in January 2024. Histopathologically, the nail bed mass was
202 diagnosed as BSCC, while the lip lesion was diagnosed as BISC. Therefore, FcaPV3 and FcaPV4 exhibit
203 distinct tissue tropisms and tumor associations, similar to the site-specific pathogenicity observed in
204 PVs of humans and other animals.
205 Comparative genomic analysis of FcaPV3 sequences identified from a nail bed mass that developed in
206 June 2023 (GenBank accession number LC859345.2) and from an inflammatory nail bed lesion that
207 appeared 252 days later in January 2024 (GenBank accession number LC884935.1) showed 23
208 nucleotide differences across 7,583 bases. These findings suggest two possibilities—the same strain
209 evolved over the 252-day period, or a different strain, distinct from the one detected in August 2023,
210 subsequently infected the cat. We consider the first possibility more likely, as FcaPV3 was detected in
211 lesions located near each other in the same cat. Although DNA viruses are typically considered to have
212 greater genomic stability than RNA viruses, this observation suggests that FcaPV3 may undergo more
213 rapid evolution than previously recognized.
214 In the evolution of human papillomaviruses (HPVs), APOBEC3 proteins play a well-documented role
215 [32]. The accumulation of C-to-T substitutions is a hallmark of HPV evolution driven by APOBEC3-
216 mediated mutagenesis. Moreover, a high burden of APOBEC3-induced mutations in HPV genomes has
217 been associated with an increased probability of tumor regression [34]. To date, the role of feline
218 APOBEC3 in the genomic evolution of FcaPV has not been reported. However, the numerous C-to-T
219 substitutions observed in this case suggest a potential relationship similar to that seen between human
220 APOBEC3 and HPV. Further virological and cellular studies are warranted to elucidate this relationship.
221 Co-infection involving different PV types has been documented in several species, including humans,
222 dogs, cattle, and porcupines [3, 12, 13, 23, 26, 28]. In humans, multiple HPV infections were observed
223 in 105 of 178 HPV-positive individuals (59%) [23]. In dogs, canine papillomaviruses (CPV) 1 and 2 are
224 the predominant types, with CPV1 primarily associated with oral lesions and CPV2 with cutaneous
225 papillomas; co-infection with both types occurs in approximately 20% of CPV-positive cases [12]. In
226 cattle, bovine papillomaviruses (BPV) 1 and 2 frequently co-infect the same host, with all tested samples

227 showing at least dual infection [26]. Similarly, North American porcupines have been found to harbor
228 co-infection with *Erethizon dorsatum papillomavirus* 1 and 2 [13].
229 In contrast, papillomavirus infections in cats have thus far been reported only as single-type infections.
230 Therefore, the present case, in which co-infection with FcaPV3 and FcaPV4 was identified, represents
231 the first documented instance of dual papillomavirus infection in a cat.
232 Integration of HPV DNA into the host genome induces constitutive expression of the viral oncogenes
233 E6 and E7 [5, 31], which promote degradation of the host tumor suppressor proteins p53 and pRb [2,
234 10, 25, 27]. Consequently, HPV-infected cells typically show reduced p53 staining and weak-to-
235 intermediate pRb immunoreactivity. In this case, p53 staining was negative or weakly positive, and pRb
236 showed weak positivity.
237 The p53 protein regulates the cellular response to DNA damage by inducing cell cycle arrest and
238 apoptosis, whereas pRb acts as a brake on cell cycle progression by binding to E2F, a transcription factor
239 that drives cell proliferation. Suppression of these tumor suppressor proteins by viral oncoproteins leads
240 to uncontrolled cell proliferation. In this study, PCR analysis detected E6 and E7 genes of FcaPV3 and
241 FcaPV4, indicating active viral infection and possible integration of viral genomes into host cells. The
242 cat in this case was noted to habitually bite its claws, which may have caused minor wounds serving as
243 portals of viral entry. The absence or weak expression of p53, together with weak pRb staining and the
244 detection of E6 genes from FcaPV3 and FcaPV4 in tumor cells, collectively suggest degradation of
245 tumor suppressor proteins resulting from viral genome integration.
246 Previous studies have reported associations between specific FcaPV types and distinct histopathological
247 features [21]. In FcaPV3-associated lesions, tumor cells often contain abundant clear cytoplasm with
248 elongated amphophilic to basophilic intracytoplasmic inclusion bodies [21]. In contrast, FcaPV4-
249 associated lesions are characterized by cells with finely granular blue-gray cytoplasm and peripherally
250 located nuclei within hyperplastic regions [21]. In this case, rod-shaped basophilic intracytoplasmic
251 inclusions were observed in tumor cells within multiple nail bed masses where FcaPV3 DNA was
252 detected, consistent with previous findings. Similarly, tumor cells in the FcaPV4-positive lip lesion
253 exhibited grayish-blue cytoplasmic swelling characteristic of FcaPV4 infection.

p16 is a tumor suppressor that inhibits cyclin-dependent kinases (CDKs). Under normal conditions, CDKs phosphorylate pRb during the G1 phase, releasing E2F and allowing entry into the S-phase. Notably, p16 regulates cell proliferation through a negative feedback loop with pRb. In papillomavirus-induced oncogenesis, viral E7 inactivates pRb by competing with CDKs, thereby disrupting this regulatory mechanism. Consequently, p16 becomes overexpressed while cell proliferation continues unchecked, making p16 a sensitive surrogate marker of papillomavirus infection [4, 10, 11]. In this case, p16 expression was confined to tumor areas, supporting the involvement of FcaPV based on immunohistochemical findings. In contrast, p63, a basal epithelial cell marker, is expressed in tissues such as the cervix, urothelium, mammary gland, and prostate [9, 29, 30]. Strong nuclear positivity for p63 in tumor cells indicates a basal epithelial origin.

In conclusion, the multiple nail bed masses consisted of basal cell-like cells with focal squamous differentiation and intranuclear inclusion bodies, consistent with BSCC associated with FcaPV3. The lip lesion exhibited well-defined neoplastic proliferation within the epidermis, consistent with BISC associated with FcaPV4. Both neoplasms showed strong p16 immunoreactivity and weak or absent staining for pRb and p53. *In situ* hybridization confirmed the presence of the FcaPV3 and FcaPV4 E6 genes in the BSCC and BISC, respectively. According to the available literature, this is the first report of malignant tumors independently induced by FcaPV3 and FcaPV4 in a cat. Further studies are necessary to understand the pathogenesis of paFcaPV infection in cats.

DATA AVAILABILITY

The data that support the findings of this study are available from the corresponding author upon reasonable request.

CONFLICT OF INTEREST

The authors declare no conflict of interest.

ACKOWLENGMENTS

The authors thank Ms. Tomoko Nishiuchi, Ms. Miki Kawano, Ms. Natsumi Matsubara, and the staff of CADIC, University of Miyazaki.

FUNDINGS

This work was supported by grants from the Japan Agency for Medical Research and Development (AMED) Research Program on HIV/AIDS JP25fk0410075h0001, JP24fk0410047, JP25fk0410056, and JP25fk0410058 (to A.S.); the AMED Research Program on Emerging and Re-emerging Infectious Diseases JP23fk0108583, and JP24fk0108907h0001 (to A.S.); the AMED the Research Project for Practical Applications of Regenerative Medicine JP24bk0104177 (to A.S.); the AMED Program for Accelerating Medical Research JP256f0137007j0001 (to A.S. and N.F.); the JSPS KAKENHI Grant-in-Aid for Scientific Research (C) JP24K09227 (to A.S.); the JSPS KAKENHI Grant-in-Aid for Scientific Research (B) JP22H02500 (to A.S.) and JP21H02361 (to A.S.); the JSPS Bilateral Program JPJSBP120245706 (to A.S.); the JSPS Fund for the Promotion of Joint International Research (International Leading Research) JP23K20041 (to A.S.); the G-7 Grants (2024) (to A.S.); Shionogi infectious disease research promotion foundation (2024) (to A.S.); and the Ito Foundation Research Grant R6 KEN119 (to A.S.) and R6 KEN161 (to N.F.). This study was supported by the Frontier Science Research Center, University of Miyazaki.

297 **Figure Legends**

298 **Figure 1. Gross findings of the case specimens.**

299 (A) Multiple nail bed masses on the first digit of the left forelimb (**left**), second digit of the left forelimb

300 (**center**), and second digit of the left hindlimb (**right**).

301 (B) Single nail bed lesion on the second digit of the right forelimb (arrow).

302 (C) Ulcerated tumor on the left lip (arrow).

303

304 **Figure 2. Detection of *Feline catus* papillomavirus (FcaPV)**.

305 DNA was extracted from multiple nail bed masses or a lip lesion and analyzed by SYBR Green-based

306 qPCR using primers specific for FcaPV1–6 and the *Felis catus albumin* gene as a positive control.

307 Infection was assigned to the FcaPV type with the lowest Ct value.

308

309 **Figure 3. Genetic analysis of FcaPV genomes.**

310 (A) Phylogenetic tree of FcaPV3 strains generated using MUSCLE algorithm and constructed by

311 maximum likelihood and neighbor-joining methods with the Jones–Taylor–Thornton model in MEGA

312 11.

313 (B) Phylogenetic tree of FcaPV4 strains constructed as in (A).

314 (C) Partial sequence alignment of FcaPV3 detected from multiple nail bed masses in August 2023 and

315 a single nail bed lesion in February 2024.

316

317 **Figure 4. Histopathological findings of the case specimens.**

318 (A) Basosquamous cell carcinoma (BSCC), digit. Neoplastic cells infiltrate from the dermis into

319 subcutaneous tissue. Hematoxylin and eosin (HE).

320 (B) BSCC showing basal cell-like cuboidal tumor cells arranged in islands, bands, and cords with focal

321 squamous differentiation. HE.

322 (C) BSCC displaying koilocytosis with perinuclear vacuolation (arrows). HE.

323 (D) BSCC tumor cells containing rod-shaped cytoplasmic inclusion bodies (arrows). HE.

(E) Bowenoid *in situ* carcinoma (BISC), lip. Well-demarcated neoplastic proliferation confined to the epidermis, extending toward the dermis. HE.

(F) BISC tumor cells with irregular shape and indistinct borders. HE.

(G) BISC tumor cells containing grayish-blue nuclear inclusion bodies (arrows). HE.

(H) BISC tumor cells showing blue-gray cytoplasmic swelling (arrow). HE.

Figure 5. Immunohistochemical findings of the case specimens.

(A) Basosquamous cell carcinoma (BSCC) showing strong nuclear and cytoplasmic p16 immunoreactivity in tumor cells. Immunohistochemistry (IHC).

(B) Bowenoid *in situ* carcinoma (BISC) showing strong nuclear and cytoplasmic p16 immunoreactivity. IHC.

(C) BSCC showing strong nuclear p63 immunoreactivity. IHC.

(D) BISC showing strong nuclear p63 immunoreactivity. IHC.

(E) BSCC with nuclear pRb immunoreactivity in a subset of tumor cells (arrows). IHC.

(F) BISC with nuclear pRb immunoreactivity in a subset of tumor cells (arrows). IHC.

(G) BSCC tumor cells negative for p53. IHC.

(H) BISC tumor cells showing weak nuclear p53 immunoreactivity in a subset of cells (arrows). IHC.

Figure 6. *In situ* hybridization of the case specimens.

(A) Basosquamous cell carcinoma (BSCC) showing intense punctate nuclear and cytoplasmic hybridization signals for FcaPV3 E6 gene in tumor cells.

(B) Bowenoid *in situ* carcinoma (BISC) showing intense punctate nuclear and cytoplasmic hybridization signals for FcaPV4 E6 gene in tumor cells.

349 **Reference**

350 1. Altamura, G., Cuccaro, B., Eleni, C., Strohmayer, C., Brandt, S. and Borzacchiello, G. 2022.
351 Investigation of multiple Felis catus papillomavirus types (-1/-2/-3/-4/-5/-6) DNAs in feline oral
352 squamous cell carcinoma: a multicentric study. *J Vet Med Sci*. **84**: 881–884.

353 2. Boyer, S. N., Wazer, D. E. and Band, V. 1996. E7 protein of human papilloma virus-16 induces
354 degradation of retinoblastoma protein through the ubiquitin-proteasome pathway. *Cancer Res*. **56**:
355 4620–4624.

356 3. Carvalho, C. C. R., Batista, M. V. A., Silva, M. a. R., Balbino, V. Q. and Freitas, A. C. 2012.
357 Detection of bovine papillomavirus types, co-infection and a putative new BPV11 subtype in cattle.
358 *Transbound Emerg Dis*. **59**: 441–447.

359 4. Cunningham, L. L., Pagano, G. M., Li, M., Tandon, R., Holm, S. W., White, D. K. and Lele, S. M.
360 2006. Overexpression of p16INK4 is a reliable marker of human papillomavirus-induced oral high-
361 grade squamous dysplasia. *Oral Surg Oral Med Oral Pathol Oral Radiol Endod*. **102**: 77–81.

362 5. Doorbar, J. 2005. The papillomavirus life cycle. *J Clin Virol*. **32 Suppl 1**: S7-15.

363 6. Doorbar, J., Quint, W., Banks, L., Bravo, I. G., Stoler, M., Broker, T. R. and Stanley, M. A. 2012.
364 The biology and life-cycle of human papillomaviruses. *Vaccine*. **30 Suppl 5**: F55-70.

365 7. Dunowska, M., Munday, J. S., Laurie, R. E. and Hills, S. F. K. 2014. Genomic characterisation of
366 Felis catus papillomavirus 4, a novel papillomavirus detected in the oral cavity of a domestic cat.
367 *Virus Genes*. **48**: 111–119.

368 8. Graham, S. V. 2017. The human papillomavirus replication cycle, and its links to cancer
369 progression: a comprehensive review. *Clin Sci (Lond)*. **131**: 2201–2221.

370 9. Houghton, O. and McCluggage, W. G. 2009. The expression and diagnostic utility of p63 in the
371 female genital tract. *Adv Anat Pathol*. **16**: 316–321.

372 10. Ito, S., Chambers, J. K., Sumi, A., Yamashita-Kawanishi, N., Omachi, T., Haga, T., Nakayama, H.
373 and Uchida, K. 2022. Involvement of Felis catus papillomavirus type 2 in the tumorigenesis of
374 feline Merkel cell carcinoma. *Vet Pathol*. **59**: 63–74.

375 11. Klaes, R., Friedrich, T., Spitkovsky, D., Ridder, R., Rudy, W., Petry, U., Dallenbach-Hellweg, G.,
376 Schmidt, D. and von Knebel Doeberitz, M. 2001. Overexpression of p16(INK4A) as a specific
377 marker for dysplastic and neoplastic epithelial cells of the cervix uteri. *Int J Cancer*. **92**: 276–284.
378 12. Lange, C. E., Jennings, S. H., Diallo, A. and Lyons, J. 2019. Canine papillomavirus types 1 and 2
379 in classical papillomas: High abundance, different morphological associations and frequent co-
380 infections. *Vet J*. **250**: 1–5.
381 13. Mack, Z. E., Caserta, L. C., Renshaw, R. W., Nakagun, S., Gerdes, R. S., Diel, D. G., Childs-
382 Sanford, S. E. and Peters-Kennedy, J. 2023. Histopathologic and molecular characterization of
383 Erethizon dorsatum papillomavirus 1 and Erethizon dorsatum papillomavirus 2 infection in North
384 American porcupines (Erethizon dorsatum). *Vet Pathol*. **60**: 898–904.
385 14. Mazzei, M., Forzan, M., Carlucci, V., Anfossi, A. G., Alberti, A., Albanese, F., Binanti, D., Millanta,
386 F., Baroncini, L., Pirone, A. and Abramo, F. 2018. A study of multiple Felis catus papillomavirus
387 types (1, 2, 3, 4) in cat skin lesions in Italy by quantitative PCR. *J Feline Med Surg*. **20**: 772–779.
388 15. McBride, A. A. 2013. The papillomavirus E2 proteins. *Virology*. **445**: 57–79.
389 16. Medeiros-Fonseca, B., Faustino-Rocha, A. I., Medeiros, R., Oliveira, P. A. and Gil da Costa, R. M.
390 2023. Canine and feline papillomaviruses: an update. *Front Vet Sci*. **10**: 1174673.
391 17. Munday, J. S. 2014. Bovine and human papillomaviruses: a comparative review. *Vet Pathol*. **51**:
392 1063–1075.
393 18. Munday, J. S. 2014. Papillomaviruses in felids. *Vet J*. **199**: 340–347.
394 19. Munday, J. S., French, A. and Thomson, N. 2017. Detection of DNA sequences from a novel
395 papillomavirus in a feline basal cell carcinoma. *Vet Dermatol*. **28**: 236-e60.
396 20. Munday, J. S. and Knight, C. G. 2024. Papillomaviruses and Papillomaviral Disease in Dogs and
397 Cats: A Comprehensive Review. *Pathogens*. **13**: 1057.
398 21. Munday, J. S. and Thomson, N. A. 2021. Papillomaviruses in Domestic Cats. *Viruses*. **13**: 1664.
399 22. Munday, J. S., Thomson, N. A. and Luff, J. A. 2017. Papillomaviruses in dogs and cats. *Vet J*. **225**:
400 23–31.
401 23. Oyervides-Muñoz, M. A., Pérez-Maya, A. A., Sánchez-Domínguez, C. N., Berlanga-Garza, A.,
402 Antonio-Macedo, M., Valdéz-Chapa, L. D., Cerda-Flores, R. M., Trevino, V., Barrera-Saldaña, H.

403 A. and Garza-Rodríguez, M. L. 2020. Multiple HPV Infections and Viral Load Association in
404 Persistent Cervical Lesions in Mexican Women. *Viruses*. **12**: 380.
405 24. Ozbun, M. A. 2002. Human papillomavirus type 31b infection of human keratinocytes and the onset
406 of early transcription. *J Virol*. **76**: 11291–11300.
407 25. Parry, D., Bates, S., Mann, D. J. and Peters, G. 1995. Lack of cyclin D-Cdk complexes in Rb-
408 negative cells correlates with high levels of p16INK4/MTS1 tumour suppressor gene product.
409 *EMBO J*. **14**: 503–511.
410 26. Santos, E. U. D., Silva, M. a. R., Pontes, N. E., Coutinho, L. C. A., Paiva, S. S. L., Castro, R. S. and
411 Freitas, A. C. 2016. Detection of Different Bovine Papillomavirus Types and Co-infection in
412 Bloodstream of Cattle. *Transbound Emerg Dis*. **63**: e103-108.
413 27. Scheffner, M., Werness, B. A., Huibregtse, J. M., Levine, A. J. and Howley, P. M. 1990. The E6
414 oncoprotein encoded by human papillomavirus types 16 and 18 promotes the degradation of p53.
415 *Cell*. **63**: 1129–1136.
416 28. Schindler, S., Magalhães, R. A., Costa, E. L. F. and Brites, C. 2022. Genital Cytokines in
417 HIV/Human Papillomavirus Co-Infection: A Systematic Review. *AIDS Res Hum Retroviruses*. **38**:
418 683–691.
419 29. Steurer, S., Riemann, C., Büscheck, F., Luebke, A. M., Kluth, M., Hube-Magg, C., Hinsch, A.,
420 Höflmayer, D., Weidemann, S., Fraune, C., Möller, K., Menz, A., Fisch, M., Rink, M., Bernreuther,
421 C., Lebok, P., Clauditz, T. S., Sauter, G., Uhlig, R., Wilczak, W., Dum, D., Simon, R., Minner, S.,
422 Burandt, E., Krech, R., Krech, T. and Marx, A. H. 2021. p63 expression in human tumors and normal
423 tissues: a tissue microarray study on 10,200 tumors. *Biomark Res*. **9**: 7.
424 30. Sumi, A., Chambers, J. K., Ito, S., Kojima, K., Omachi, T., Doi, M. and Uchida, K. 2024. Different
425 expression patterns of p63 and p73 in Felis catus papillomavirus type 2-associated feline Merkel
426 cell carcinomas and other epidermal carcinomas. *J Vet Med Sci*. **86**: 39–48.
427 31. Vascellari, M., Mazzei, M., Zanardello, C., Melchiotti, E., Albanese, F., Forzan, M., Croce, M. F.,
428 Alberti, A. and Abramo, F. 2019. Felis catus Papillomavirus Types 1, 2, 3, 4, and 5 in Feline
429 Bowenoid *in Situ* Carcinoma: An *In Situ* Hybridization Study. *Vet Pathol*. **56**: 818–825.

430 32. Warren, C. J., Van Doorslaer, K., Pandey, A., Espinosa, J. M. and Pyeon, D. 2015. Role of the host
431 restriction factor APOBEC3 on papillomavirus evolution. *Virus Evol*. **1**: vev015.
432 33. Westra, W. H. 2014. Detection of human papillomavirus (HPV) in clinical samples: evolving
433 methods and strategies for the accurate determination of HPV status of head and neck carcinomas.
434 *Oral Oncol*. **50**: 771–779.
435 34. Zhu, B., Xiao, Y., Yeager, M., Clifford, G., Wentzensen, N., Cullen, M., Boland, J. F., Bass, S.,
436 Steinberg, M. K., Raine-Bennett, T., Lee, D., Burk, R. D., Pinheiro, M., Song, L., Dean, M., Nelson,
437 C. W., Burdett, L., Yu, K., Roberson, D., Lorey, T., Franceschi, S., Castle, P. E., Walker, J., Zuna,
438 R., Schiffman, M. and Mirabello, L. 2020. Mutations in the HPV16 genome induced by APOBEC3
439 are associated with viral clearance. *Nat Commun*. **11**: 886.
440

Figure 1

A

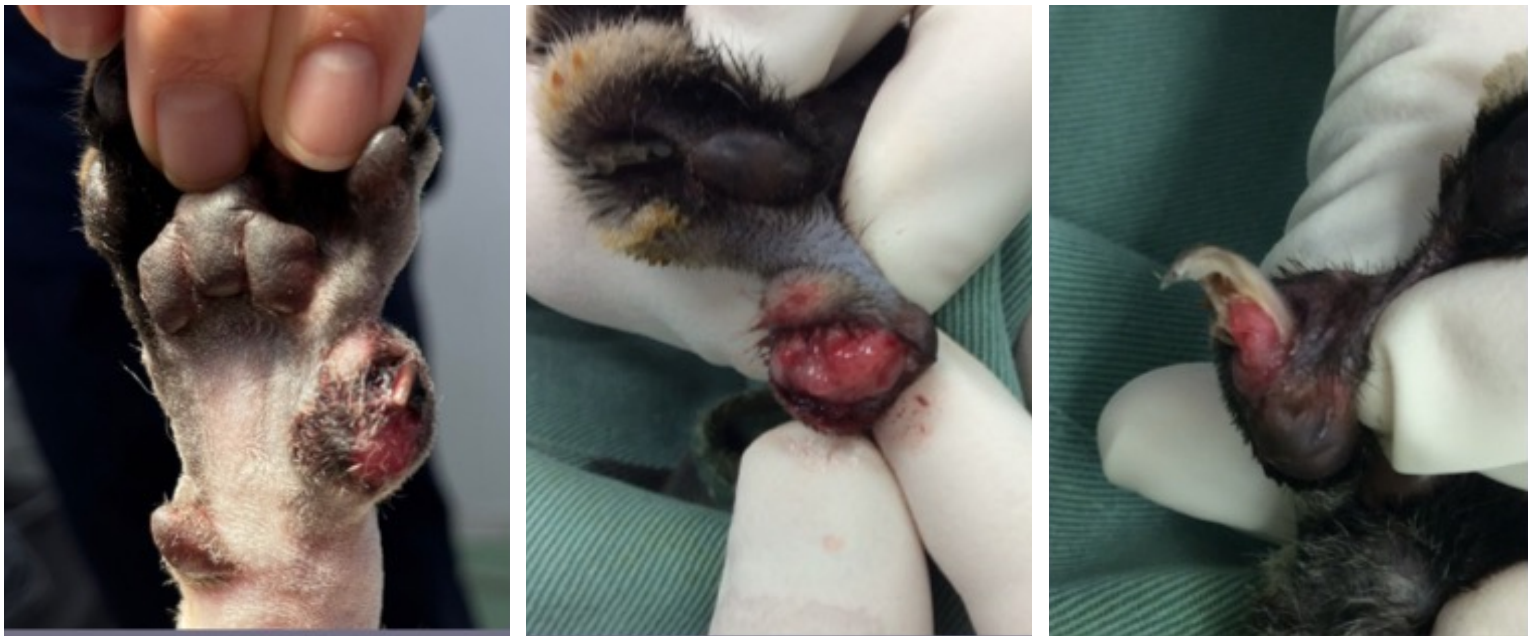

B

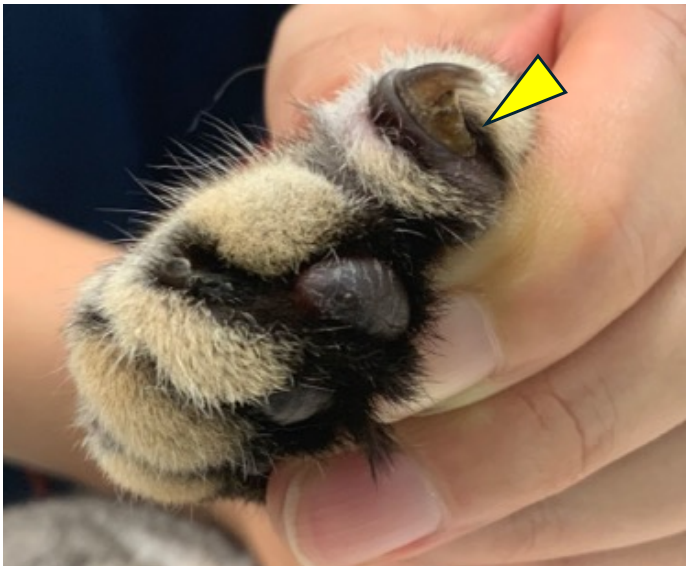

C

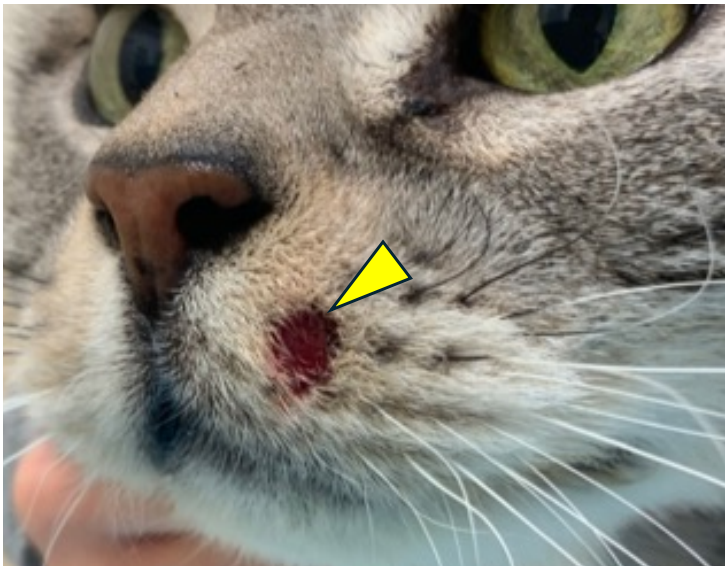

Figure 2

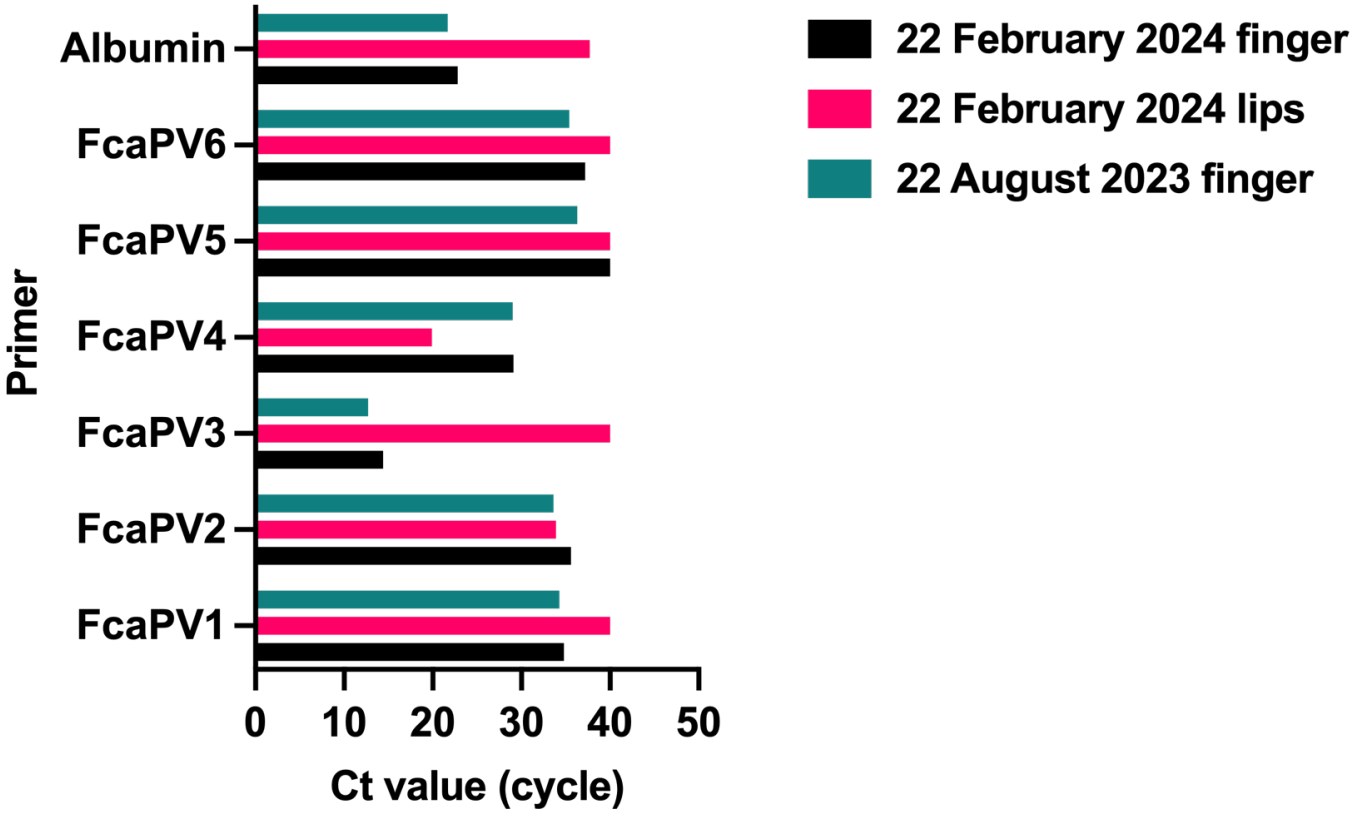
Albumin
FcaPV6
FcaPV5
FcaPV4
FcaPV3
FcaPV2
FcaPV1
Primer
0
10
20
30
40
50
Ct value (cycle)
22 February 2024 finger
22 February 2024 lips
22 August 2023 finger

Figure 3

A


KY825188.1 |USA|2012-01|Missouri
JX972168.1 |New Zealand|2010|MyDave
LC859345.2 |Japan|2023-08-22|GNGN3/Fukuoka/Japan/2023
ON226484.1 |China|2019|
LC884935.1 |Japan|2024-02-27|FcaPV3/cat/Japan/Fukuoka GNGN3/2024
ON226485.1 |China|2019|
ON226486.1 |China|2019|
0.00050

B

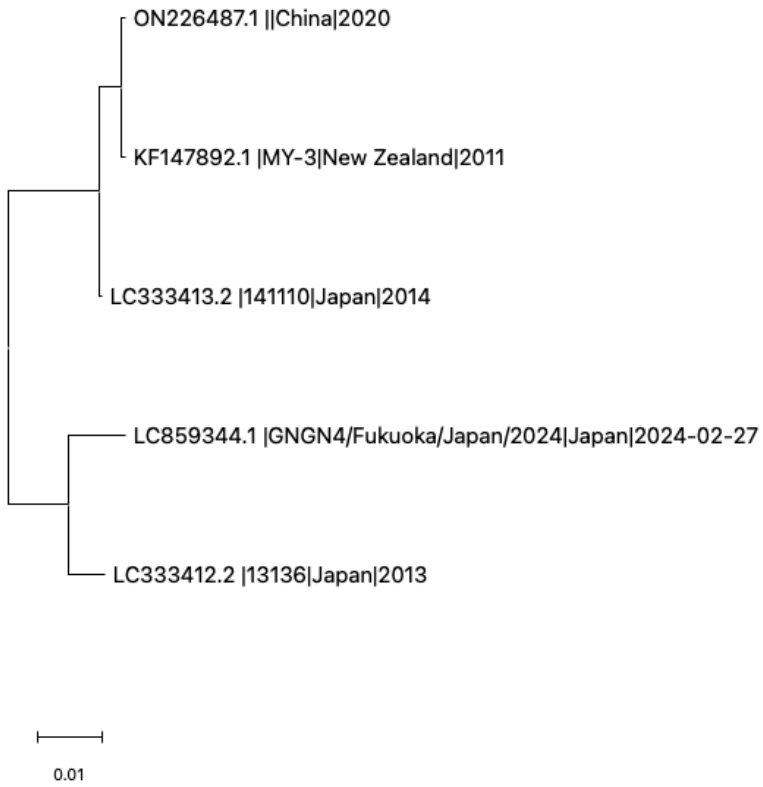
ON226487.1 ||China|2020
KF147892.1 |MY-3|New Zealand|2011
LC333413.2 |141110|Japan|2014
LC859344.1 |GNGN4/Fukuoka/Japan/2024|Japan|2024-02-27
LC333412.2 |13136|Japan|2013
0.01

Figure 3

C

Species/Abbrv	*	*	*	*	*	*	*	*	*	*	*	*	*	*	*	*	*	*	*	*	*	*	*	*	*	*	*	*	*	*	*
1. August 2023	G	C	T	T	C	A	C	T	T	T	T	A	C	C	A	G	G	A	T	C	T	C	A	G	T	A	C	T	A	T	T
2. February 2024	G	G	T	T	C	A	C	T	A	T	T	A	C	C	A	G	G	A	T	C	T	C	A	G	T	A	G	T	A	T	T

Figure 4

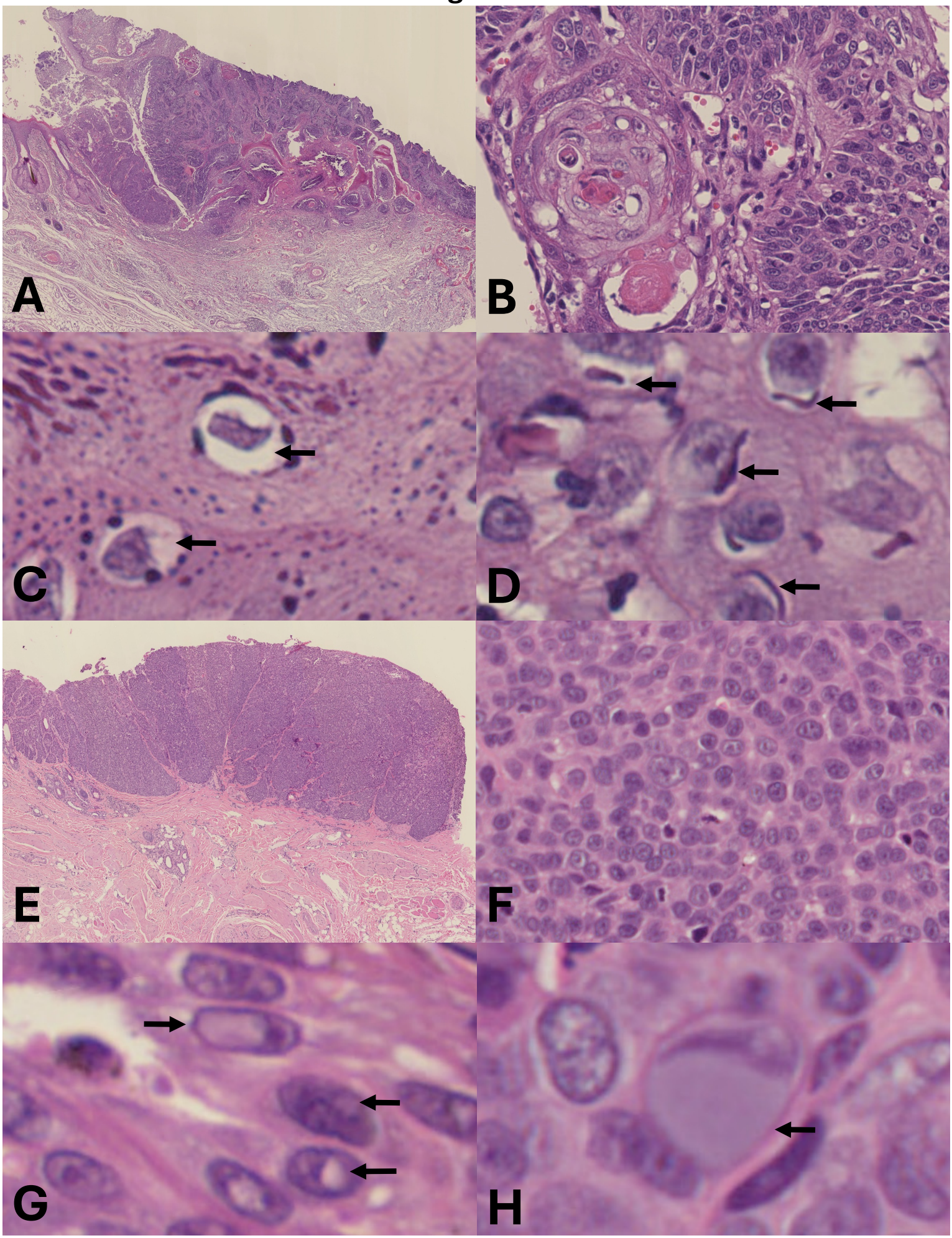

Figure 5

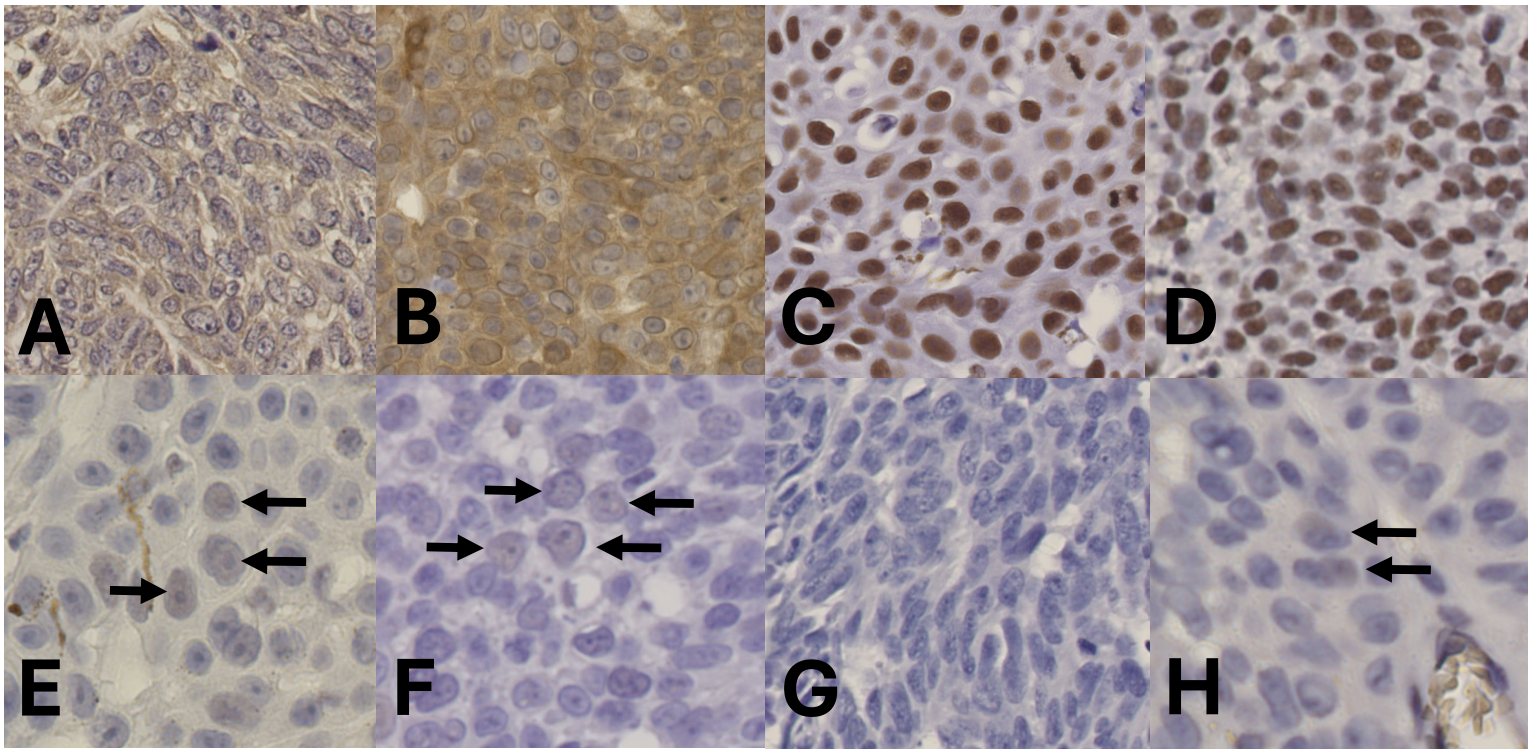

Figure 6